Results in Physics 17 (2020) 103061

Contents lists available at ScienceDirect

Results in Physics

journal homepage: www.elsevier.com/locate/rinp

Investigation of structural and physical properties of Eu^{3+} ions substituted $Ni_{0.4}Cu_{0.2}Zn_{0.4}Fe_2O_4$ spinel ferrite nanoparticles prepared via sonochemical approach

Y. Slimani[a,*], B. Unal[b], M.A. Almessiere[a], A. Demir Korkmaz[c], Sagar E. Shirsath[d], Ghulam Yasin[e], A.V. Trukhanov[f,g,h], A. Baykal[i]

[a] Department of Biophysics, Institute for Research and Medical Consultations (IRMC), Imam Abdulrahman Bin Faisal University, P.O. Box 1982, Dammam 31441, Saudi Arabia
[b] Institute of Forensic Sciences & Legal Medicine, and Institute of Nanotechnology & Biotechnology, Istanbul University–Cerrahpaşa, Buyukcekmece Campus, Alkent 2000 Mah., Buyukcekmece, Istanbul 34500, Turkey
[c] Department of Chemistry, Istanbul Medeniyet University, 34700 Istanbul, Uskudar, Turkey
[d] School of Materials Science and Engineering, University of New South Wales, Kensington, Sydney, NSW 2052, Australia
[e] State Key Laboratory of Chemical Resource Engineering, College of Materials Science and Engineering, Beijing University of Chemical Technology, Beijing 100029, China
[f] National University of Science and Technology MISiS, Moscow, Russia
[g] South Ural State University, 76, Lenin Ave., Chelyabinsk 454080, Russia
[h] SSPA "Scientific and Practical Materials Research Centre of the NAS of Belarus", 19, P. Brovki str., Minsk 220072, Belarus
[i] Department of Nanomedicine, Institute for Research and Medical Consultations (IRMC), Imam Abdulrahman Bin Faisal University, P.O. Box 1982, Dammam 31441, Saudi Arabia

ARTICLE INFO

Keywords:
Spinel ferrites
Nanomaterials
Optical properties
Magnetic properties
Dielectric properties

ABSTRACT

Green and facile process for $Ni_{0.4}Cu_{0.2}Zn_{0.4}Fe_{2-x}Eu_xO_4$ (x = 0.00–0.10) spinel ferrite nanoparticles (SNPs) prepared via ultrasonic irradiation (without any post annealing process) has been deeply investigated. The influence of Eu^{3+} substitutions on the structure, morphological, optical, magnetic, electrical and dielectric traits of NiCuZn SNPs was assessed. Tauc plots revealed direct optical band gaps in a very tight interval of 1.86–1.90 eV. Magnetization measurements exposed a superparamagnetic behavior at room temperature and below the blocking temperature (T_B) a superparamagnetic-ferromagnetic transition was noticed. The saturation magnetization (M_s) value is highest for pure $Ni_{0.4}Cu_{0.2}Zn_{0.4}Fe_2O_4$ (i.e. x = 0.00) SNP with $M_s \sim 58.9$ emu/g at room temperature. The saturation magnetization (M_s) declines with rising Eu^{3+} substituting content. AC conductivity decreases as a function of exponent power base law. Maximum variation in dc conductivity is observed to be around the substitution ratio of x = 0.02. It is found that activation energy is highly dependent on both Eu ions substitution ratios and temperature ranges. The frequency dependence of dielectric functions is explained by Koop's models based on Maxwell-Wagner theory.

Introduction

Nano-sized spinel ferrites (SNPs) are extremely popular choice for use in a variety of applications in electronics as well as communication for the latest years owing to their extraordinary magnetic, optical, electrical, and catalytic characteristics [1–4]. Researchers can tune these properties by doping with different materials to be used in sensing, magnetic resonance imaging, catalysis, and many other applications [3–12]. The nickel copper zinc ferrite is a soft ferrite with extreme permeability in the radio-frequency range, low sintering temperature, elevated Curie temperature and high electrical resistivity. Ni-Cu-Zn ferrites are principally utilized as multilayer chip inductors (MLCI) in electronics as well as inductors, transformer cores, deflection yokes, and recording heads [13–15].

Recently, investigators have examined the effects of tuning the composition of NiCuZn ferrites by either by changing the amounts of metal ions making up the formula or doping with new metals. For example, Nam et al. prepared $Ni_{0.2}Cu_xZn_{0.8-x}Fe_2O_4$ (x = 0.2–0.6) with and without acetyl acetone. They obtained spinel structures in all compositions with crystalline sizes 10–20 nm except for x = 0.6, which displayed hematite as a second phase. However, the hematite phased disappeared after applying the acetyl acetone as an additive and this

* Corresponding author.
E-mail address: yaslimani@iau.edu.sa (Y. Slimani).

https://doi.org/10.1016/j.rinp.2020.103061
Received 10 February 2020; Received in revised form 3 March 2020; Accepted 14 March 2020
Available online 17 March 2020

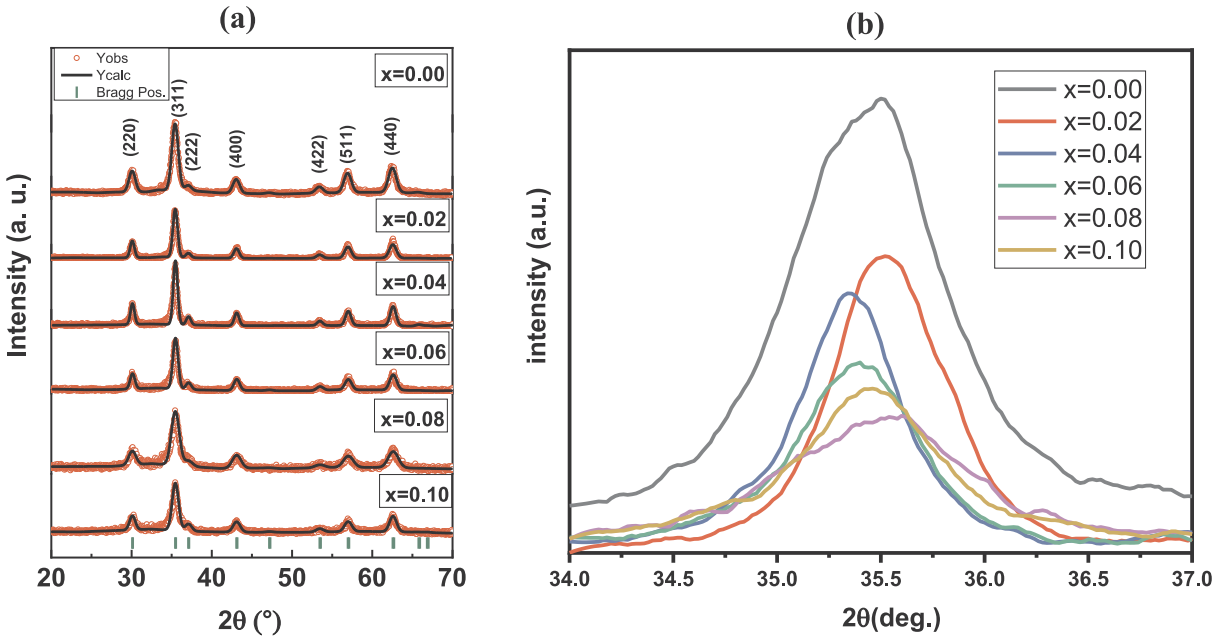

Fig. 1. (a) XRD powder patterns of $Ni_{0.4}Cu_{0.2}Zn_{0.4}Eu_xFe_{2-x}O_4$ ($0.00 \leq x \leq 0.10$) SNPs. (b) The variation in 2θ of (3 1 1) Bragg peak position with substitution of Eu.

Table 1
The refined structural parameters, cations distribution and size of magnetic nanoparticles (D_M) for $Ni_{0.4}Cu_{0.2}Zn_{0.4}Eu_xFe_{2-x}O_4$ ($0.00 \leq x \leq 0.10$) SNPs.

x	a (Å)	V (Å)^3	D_{XRD} (nm) ± 0.05	D_M(nm)	$\chi^2(chi^2)$	R_{Bragg}	Cations distribution	
							Tetrahedral A-site	Octahedral B-site
0.00	8.397(4)	592.14	22.81	21.62	1.36	2.73	$Zn_{0.4}Fe_{0.6}$	$Ni_{0.4}Cu_{0.2}Fe_{1.4}$
0.02	8.399(1)	592.52	14.94	13.88	1.21	1.36	$Zn_{0.4}Fe_{0.6}$	$Ni_{0.4}Cu_{0.2}Eu_{0.02}Fe_{1.38}$
0.04	8.404(3)	593.33	12.59	11.78	1.68	4.73	$Zn_{0.4}Fe_{0.6}$	$Ni_{0.4}Cu_{0.2}Eu_{0.04}Fe_{1.36}$
0.06	8.404(6)	593.67	11.12	10.34	1.30	3.55	$Ni_{0.01}Zn_{0.4}Fe_{0.59}$	$Ni_{0.39}Cu_{0.2}Eu_{0.06}Fe_{1.35}$
0.08	8.413(1)	595.48	10.16	9.85	1.16	6.80	$Ni_{0.02}Zn_{0.4}Fe_{0.58}$	$Ni_{0.38}Cu_{0.2}Eu_{0.08}Fe_{1.34}$
0.10	8.415(2)	595.91	6.99	6.51	1.37	4.36	$Ni_{0.04}Zn_{0.4}Fe_{0.56}$	$Ni_{0.36}Cu_{0.2}Eu_{0.1}Fe_{1.34}$

sample exhibited the highest saturation magnetization (*Ms*) of at RT and 77 K. $Ni_{1-x}Zn_xFe_2O_4$ ferrite samples with × up to 1.0 were produced in a study by Shinde and co-workers [16]. The results revealed that the the Curie temperature decreased with growing zinc content whereas *Ms* improved up to x = 0.4 but reduced as the amount of zinc was further increased. In a research paper by Azhagushanmugam and co-workers [17] explored the consequence of the sintering temperature on the crystal structure of $Ni_{0.6}Zn_{0.4}Fe_2O_4$ obtained by co-precipitation. They found that the crystal sizes increased from 45.59 to 50.47 nm with rising the sintering temperature from 130 to 900 °C. There were also studies on the substitution of metal ions NiCuZn ferrites by different metal ions. For example, Hashim et al. [18] studied the incorporation of In^{3+} as a replacement for Fe^{3+} in NiCuZn ferrites. The rise in the molar ratio of indium caused a loss in *Ms* due to the replacement of In^{3+} of 0 μ_B ions in Fe^{3+} of 5μ_B ions and a lessening in dielectric loss tangent (tan δ) since the In^{3+} increased the grain's resistance by limiting the hopping mechanism between the ferrous ion and the ferric ion. In another study, Saida and coworkers [19] have investigated the impact of cobalt substitution on nickel, zinc, and copper ions separately in $Ni_{0.4}Cu_{0.2}Zn_{0.4}Fe_2O_4$. The magnetic properties were elevated by substitution of cobalt into the crystal structure. Their X-ray diffraction (XRD) studies demonstrated that the lattice parameter diminished as the amount of cobalt increased in general while there was an increment in *Ms* as the crystallite size of samples raised following a sintering treatment. Eltabey et al. [20] added Al^{3+} as a substituent for ferric ion in $Ni_{0.4}Cu_{0.2}Zn_{0.4}Fe_{2-x}Al_xO_4$ and found that the substitution of the ferric ion caused the M_s, initial permeability (μ_i), and the dc electrical resistivity (ρ) enhance with rising × up to 0.05, however the M_s and μ_i decreased when x > 0.05. The rare earth metal (RE) ions, on the other hand, are known to enhance the optical properties and tune the magnetic features of ferrites with spinel structures. For instance, Roy et al. [21] examined how the La^{3+} substitution in Fe^{3+} affected the triats of NiCuZn ferrites with a formula $(Ni_{0.25}Cu_{0.20}Zn_{0.55})Fe_{2-x}La_xO_4$ where x ≤ 0.075. As the La substitution amplified up to x = 0.025, magnetic loss decreased while the AC resistivity and the permeability increased. The *Ms* and the coercivity also rised up to x = 0.025 and then diminished. Kabbur et al. [22] described the effect of substituting smaller Fe^{3+} with larger Tb^{3+} on the electrical and magnetic traits of $Ni_{0.25}Cu_{0.30}Zn_{0.45}Tb_xFe_{2-x}O_4$ (x ≤ 0.125). Increasing the concentration of Tb^{3+} resulted in a loss in μ_i owing to spin canting by the paramagnetic Tb^{3+} ions and a decrease in *Ms* based on the fact that the larger Tb^{3+} ions distorting the structure and the magnetization. Some of the studies on Ni-Cu-Zn ferrites have found that using setting the molar ratio of Cu = 0.2 results in good electrical resistivity as well as *Ms* [14,23]. Moreover, fixing the molar ratios of Zn/Ni = 1.0 provides the maximum *Ms* [14,23,24]. For that reason, a number of researchers have reported the synthesis and application of $Ni_{0.4}Cu_{0.2}Zn_{0.4}Fe_2O_4$ by diverse approaches. In a study done by Liu and co-workers [25], NiCuZn ferrite thin films were prepared for an application in radio frequency integrated inductors. Harzali and co-workers [23] reported that when the ferric ion was partially substituted with RE ions (Eu^{3+}, Sm^{3+}, Gd^{3+} and Pr^{3+}), a distortion in the microstructure of the $Ni_{0.4}Cu_{0.2}Zn_{0.4}$ ferrite and an enhancement in their magnetic properties were observed. Therefore, it is important to study the substitution of $Ni_{0.4}Cu_{0.2}Zn_{0.4}Fe_2O_4$ with other metal ions as well as RE ions for investigating their effect on the magnetic-optical features of the ferrites.

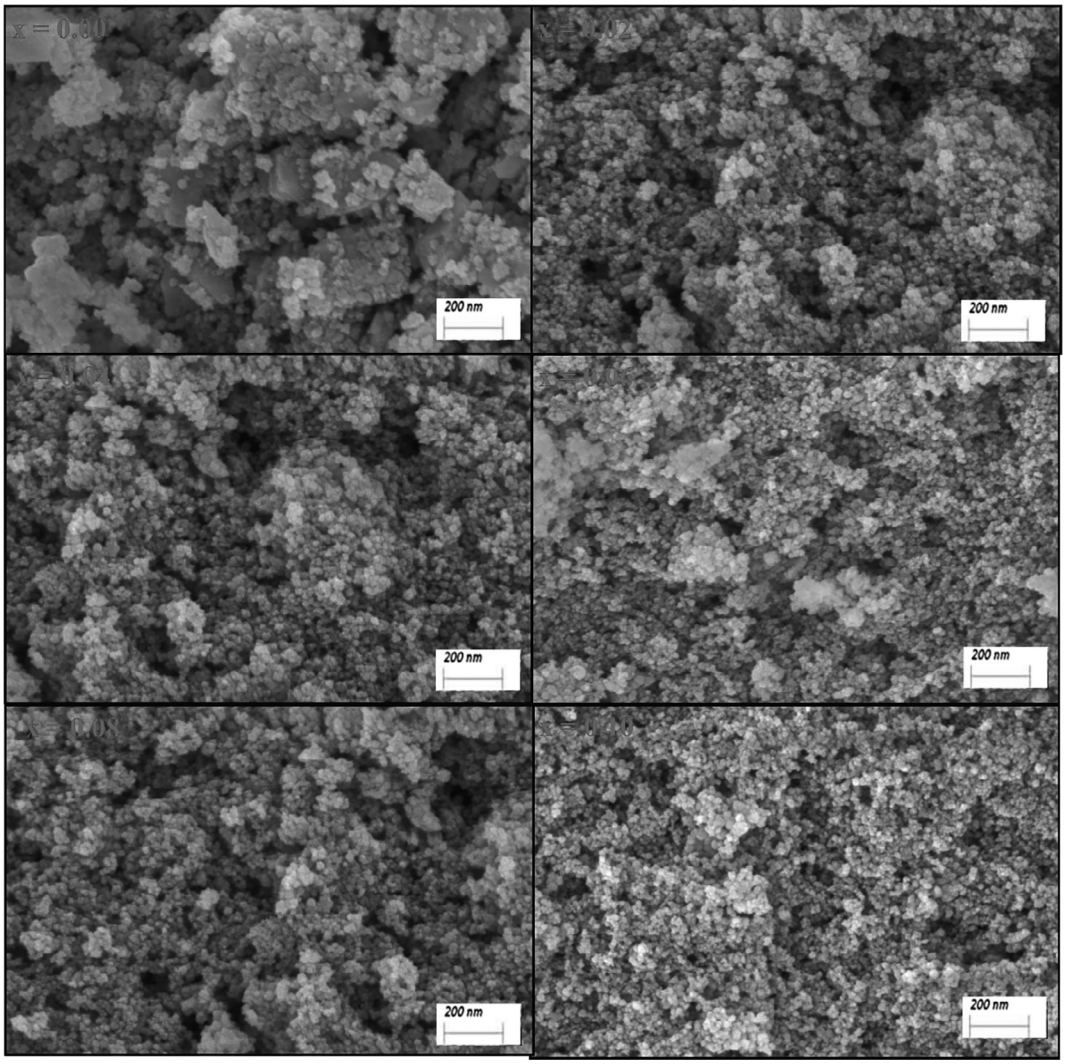

Fig. 2. SEM images of $Ni_{0.4}Cu_{0.2}Zn_{0.4}Eu_xFe_{2-x}O_4$ (x = 0.00, 0.02, 0.06 and 0.10) SNPs.

There have been no reports on the substitution of Eu^{3+} with the ferric ions into $Ni_{0.4}Cu_{0.2}Zn_{0.4}Fe_2O_4$ SNPs. Thus, we have chosen doping the nano-sized Ni-Cu-Zn ferrite ($Ni_{0.4}Cu_{0.2}Zn_{0.4}Fe_2O_4$) with rare earth europium ions. We employed ultrasound irradiation (sonochemical approach) to synthesize $Ni_{0.4}Cu_{0.2}Zn_{0.4}Fe_{2-x}Eu_xO_4$ ($x \leq 0.10$) SNPs. The sonochemistry approach is feasible in reducing the agglomeration of nanoparticles, the reaction time and the need for using large amounts of organic solvents. Therefore, we examined in this work the outcome of the substitution of Eu^{3+} on the structure, morphology and physical traits (magnetic, electrical and optical) of $Ni_{0.4}Cu_{0.2}Zn_{0.4}Fe_2O_4$ SNPs prepared with a sonochemical approach.

Experimental

All reactants were received from Alfa Aesar and used as received. In order to fabricate $Ni_{0.4}Cu_{0.2}Zn_{0.4}Fe_{2-x}Eu_xO_4$ (x = 0.00–0.10) SNPs by ultrasonic irradiation method, stoichiometric amounts of high purity metals nitrate of Zn, Ni, Eu, Cu, Fe and citric acid were mixed together in 70 ml of DI water. The pH of the sol was attuned via 2 M NaOH solution to 11 and them was exposed to ultrasonic irradiations during 30 min via UZ SONOPULS HD 2070 homogenizer (70 W and 25 kHz). Then, the mixture consisting of the final powders was washed with Deionized water. The powders parted by exterior magnet and dried at 90 °C for 24 h. All products were synthesized without any calcination.

The nano-spinal ferrite compositions were analyzed through Rigaku Miniflex powder X-ray diffraction (XRD) applied for phase examination. Morphological observations and chemical compositions were made via scanning electron microscope (SEM; FEI Titan 80–300 ST) coupled with EDX system. The microstructure was imaged by transmission electron microscopy (TEM; FEI, Morgagni 268). Electron diffraction analysis in selected area electron diffraction (SAED) mode was done. Optical investigations were investigated by means of UV–visible diffuse reflectance (DR; JASCO V-750) spectrophotometer. Magnetic characterizations were determined via a Quantum Design DynaCool PPMS. The dielectric and electrical measurements were performed by Novocontrol Alpha-N high-resolution dielectric-impedance analyzer.

Results and discussion

Structure

XRD patterns of $Ni_{0.4}Cu_{0.2}Zn_{0.4}Fe_{2-x}Eu_xO_4$ (x = 0.00 – 0.10) SNPs were illustrated in Fig. 1(a). XRD investigation of the whole ratios indicated the formation of single phase of Ni-Cu-Zn SNPs where the substitutions did not change the structure of the host material. The diffraction peaks at (2 2 0), (3 1 1), (2 2 2), (4 0 0), (4 2 2), (5 1 1) and (4 4 0) were agreed with the ICDD card no: 10–0325 of Ni spinel ferrite with cubic structure. The mean XRD peak at (3 1 1) is slightly shifted in the direction of lower diffraction angles with increasing the content of Eu as displayed in Fig. 1(b). The cell parameters, cell volume and

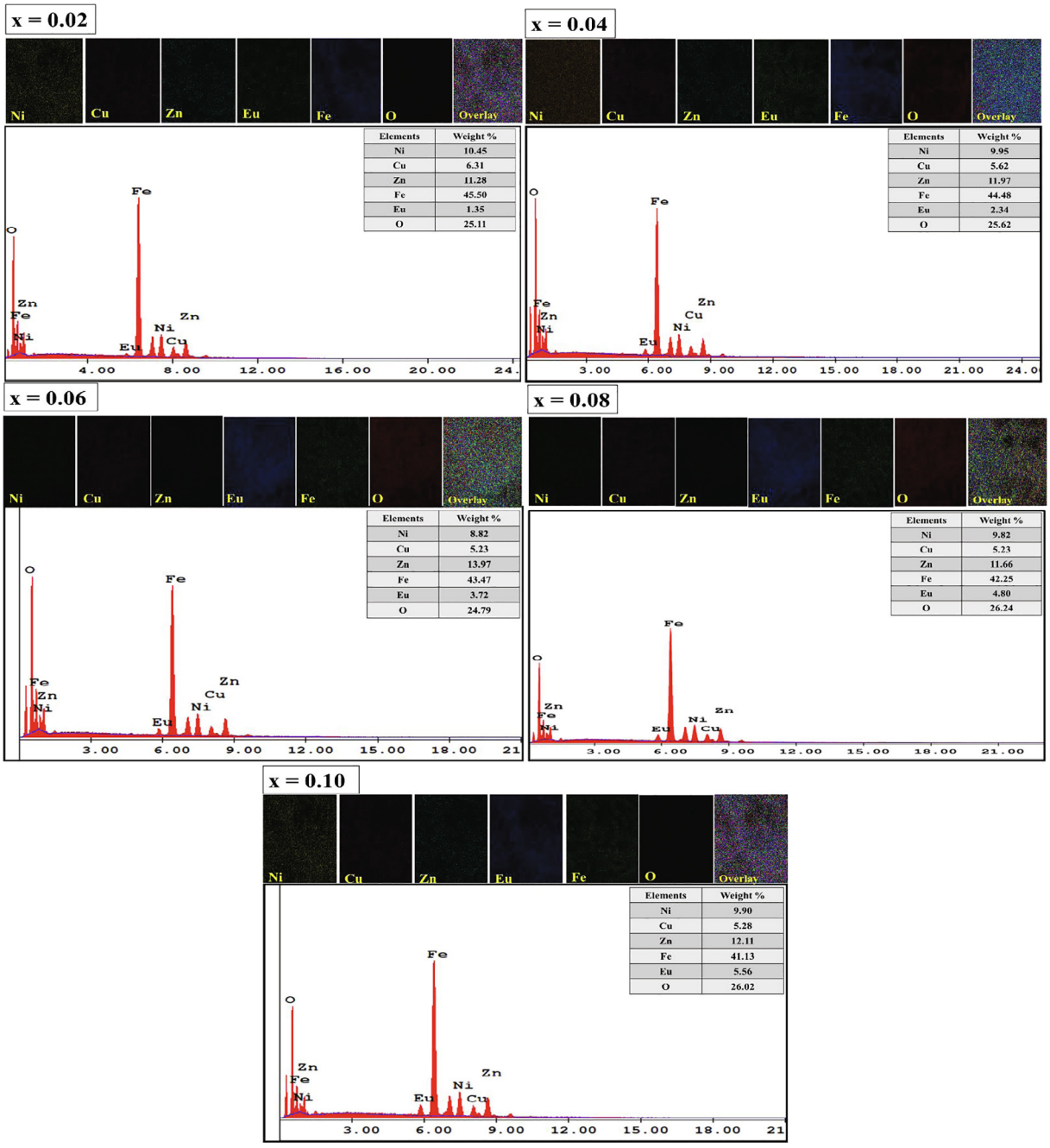

Fig. 3. EDX spectra and elemental mappings of $Ni_{0.4}Cu_{0.2}Zn_{0.4}Eu_xFe_{2-x}O_4$ (x = 0.06 and 0.10) SNPs.

average crystallite size were calculated by applying Rietveld refinement done by FullProf software (Table 1). The cell parameter 'a' increased with rising Eu^{3+} ions as a result of the enlargement in crystal due to the substitution of the octahedral sites by larger ions of Eu^{3+}. The average crystallites size was evaluated by applying Debye–Scherrer equation and it was observed to decrease from about 24 to 7 nm with increasing the ratio of Eu^{3+}.

Morphology

SEM images along with the corresponding EDX spectra and elemental mapping were presented in Figs. 2 and 3, respectively. Fig. 2 revealed accumulating cubic grains owing to the interactions between magnetic nano-grains. Elemental mappings and EDX analyses of $Ni_{0.4}Cu_{0.2}Zn_{0.4}Eu_xFe_{2-x}O_4$ (x = 0.00 – 0.10) SNPs showed the homogenized chemical composition with occurrence of the subsequent elements Zn, Fe, Ni, Eu, Cu and O. Fig. 4 shows the TEM images of the $Ni_{0.4}Cu_{0.2}Zn_{0.4}Eu_xFe_{2-x}O_4$ (x = 0.02 and 0.04) SNPs. The particles were cubic and appeared in agglomeration but in monolayer manner. The nanoparticles displayed the isolated continuous rings as shown by SAED patterns (Fig. 4), indicating the polycrystalline nature of the particles. The first six rings observed in SAED patterns agreed well with XRD patterns. The particle size distribution histogram for each specimen depicts that the average size is about 25 nm for different specimens, confirming the successful formation nano-sized particles.

Optical analysis

The % DR spectra analyses were conducted to specify optoelectronic properties of mixed $Ni_{0.4}Cu_{0.2}Zn_{0.4}Fe_{2-x}Eu_xO_4$ (x = 0.00 – 0.10) SNPs

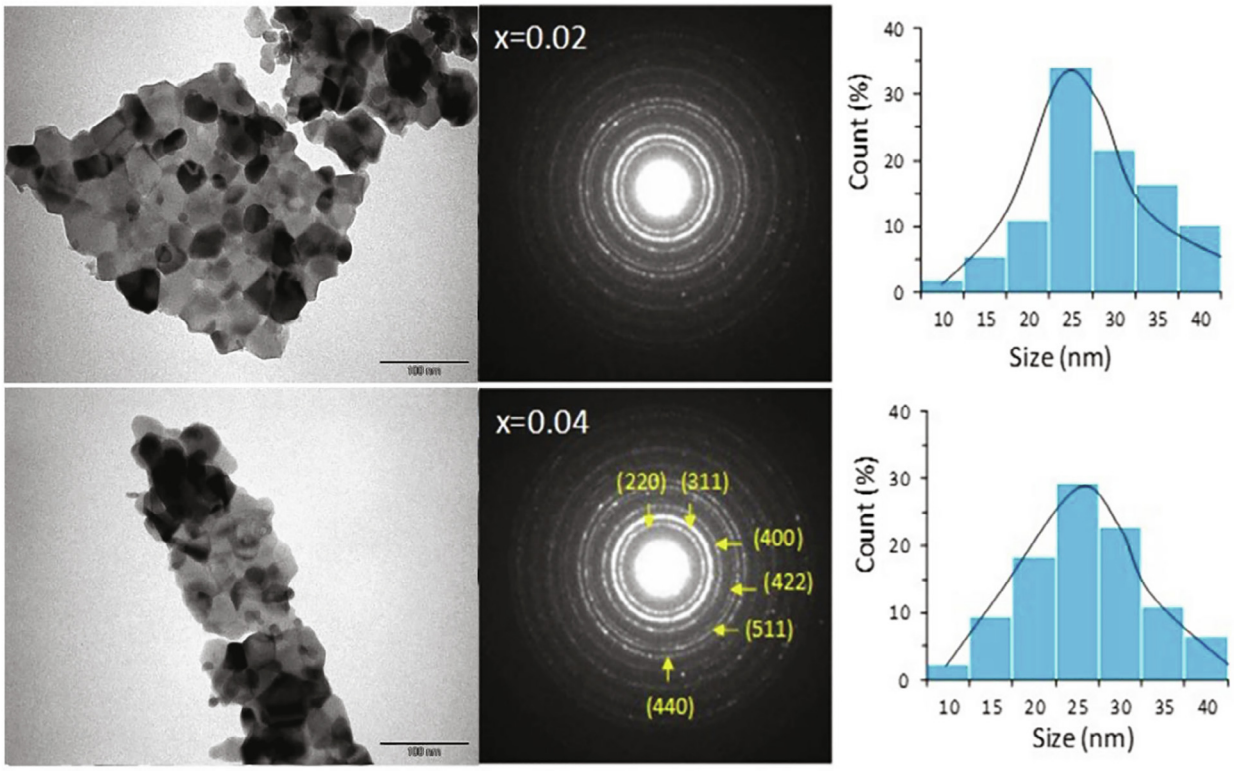

Fig. 4. TEM images, SAED patterns and particle size distribution diagrams of $Ni_{0.4}Cu_{0.2}Zn_{0.4}Eu_xFe_{2-x}O_4$ (x = 0.02 and 0.04) SNPs.

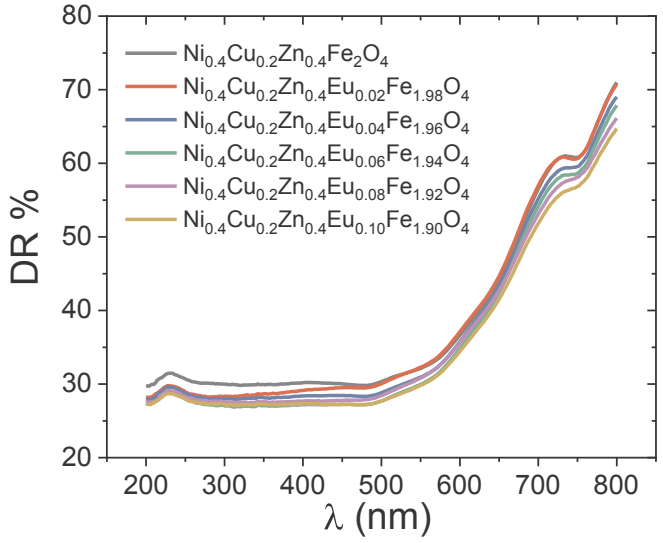

Fig. 5. % DR spectra versus of $Ni_{0.4}Cu_{0.2}Zn_{0.4}Eu_xFe_{2-x}O_4$ ($0.00 \le x \le 0.10$) SNPs in UV–Vis region.

in a wavelength interval of 200–800 nm, Fig. 5. All recorded spectra from NPs reflect the light with a magnitude between 27 and 32%. Rare earth ion doped $Ni_{0.4}Cu_{0.2}Zn_{0.4}Fe_2O_4$ SNPs have reflectance magnitudes around 30%. There is practically a linear increase excepting around 750 nm wavelength of light till maximum 71% in the following sweep range until 800 nm. The explanation of DR % data for determination of optoelectronic properties is centered on the Kubelka-Munk model and Kubelka-Munk function $F(R_\infty)$, which is directly proportional with absorption coefficient (α). Direct E_g values were projected applying the Tauc and Davis-Mott model by extrapolating the plots of $(\alpha hv)^2$ *vs* hv to the zero value for $(\alpha hv)^2$, where h is Planck's constant and v is frequency [26–29]. All plots and extrapolated band gaps belonging to $Ni_{0.4}Cu_{0.2}Zn_{0.4}Fe_{2-x}Eu_xO_4$ (x = 0.00 – 0.10) SNPs are given in Fig. 6. Undoped $Ni_{0.4}Cu_{0.2}Zn_{0.4}Fe_2O_4$ SNP has 1.86 eV direct E_g value. Eu^{3+} ion dopant concentrations with x = 0.02. 0.04, 0.06, 0.08 and 0.10 do not cause significant change from this magnitude. All doped samples have just slightly higher E_g magnitudes at maximum 1.90 eV.

Magnetic properties

Magnetization versus magnetic field (M−H)

Fig. 7 presents $M-H$ curves (magnetization versus applied magnetic field) for $Ni_{0.4}Cu_{0.2}Zn_{0.4}Fe_{2-x}Eu_xO_4$ (x = 0.00 – 0.10) SNPs. The measurements were done using VSM at RT and over an applied field between + 90 and −90 kOe. From this figure, it is evident that all the prepared NPs exhibit superparamagnetic (SPM) nature at room temperature. Hence, the SPM state could be linked with the Langevin function ($L(x)$) [30,31]:

$$M(H) = M(\infty)L(x) \quad (1)$$

Here $M(\infty)$ is the saturated magnetization. $L(x)$ is expressed as follow [30,31]:

$$L(x) = \left[\coth(x) - {}^{1}\!/_{x}\right] where\ x = \frac{M_s VH}{k_B T} \quad (2)$$

where the volume (V) is proportional to the size of magnetic spherical nanoparticles (D_M) with the following relation; $V = \frac{\pi D_M^3}{6}$. The fitting of M−H curves by equations (1) and (2), as shown in Fig. 8, will lead to determine the D_M values, which are summarized in Table 1. It is observable that the D_M values are slightly lower than the D_{XRD} values. This is frequently attributable to the magnetic dead layers on the top of crystalline cores. The non-magnetic surface layers of NPs frequently give rise to a tinier magnetic size than the physical size [31].

Fig. 9(a) and (b) show the variations in saturation magnetization (M_s) and the experimental magnetic moments (n_B), respectively. The values of n_B per unit formula in units of Bohr magneton were calculated as follow [32,33]:

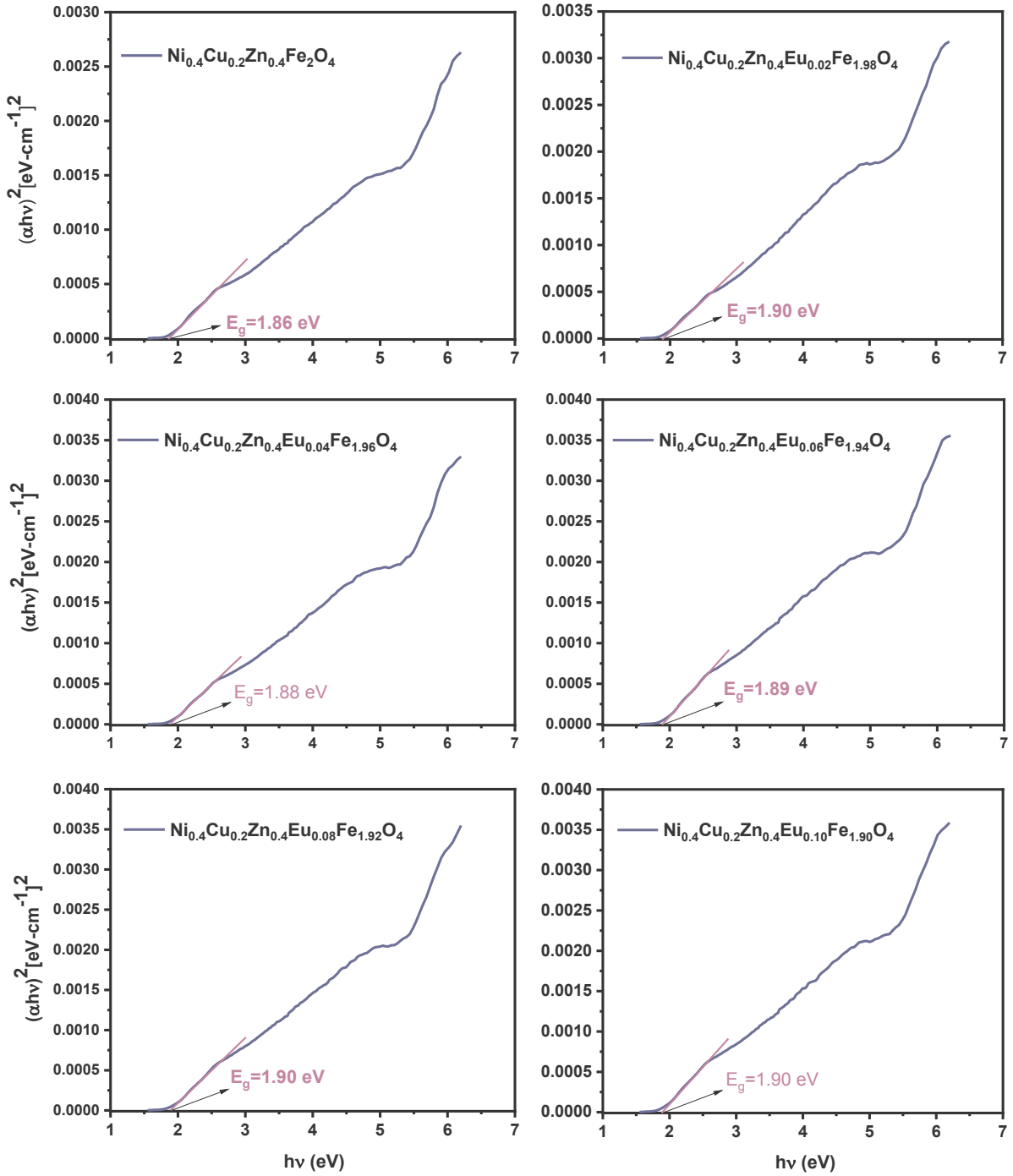

Fig. 6. Tauc plots of $Ni_{0.4}Cu_{0.2}Zn_{0.4}Eu_xFe_{2-x}O_4$ ($0.00 \leq x \leq 0.10$) SNPs. Extrapolating the straight portion of graph to hυ axis at the $(\alpha h\upsilon)^2 = 0$ determines the value of band gap.

$$n_B = \frac{Molecular weight \times M_s}{5585} \quad (3)$$

The M_s value for pure $Ni_{0.4}Cu_{0.2}Zn_{0.4}Fe_2O_4$ (i.e. × = 0.00) SNP is ~58.9 emu/g at room temperature. The present ultrasonicated NiCuZn nanoferrite displays M_s value greater than those prepared through sol–gel auto-combustion approach [34,35]. It is also higher than that found in NiCuZn thin film [36]. No enhancement in M_s magnitudes was noticed with Eu^{3+} substitution. In comparison with non-substituted sample, it is noticed that the M_s magnitude drops with the growth in Eu^{3+} content. It is recognized that variations in magnetization and D_{XRD} are proportional [37,38]. In this study, it is evident that the M_s decreases when diminishing the crystallites size as a result of Eu^{3+} substitutions. Frequently, the fall in magnetization could be accredited to the surface effect of MNPs as a result of tinier crystallites size that can be described by supposing the appearance of dead magnetic layer owing to the disorder of surface spins [39]. At the surface, it is predicted that the spins number rises when the crystallites size became tinier. Furthermore, it is expected theoretically to observe a decrease in the magnetization with Eu^{3+} substitution in NiCuZn SNPs as a result of substituting Fe^{3+} ions having magnetic moment of 5 μ_B by Eu^{3+} ions with lower magnetic moment of 3.4 μ_B. Therefore, the decrease in M_s values is principally attributed to the variance in the magnetic moments of Eu^{3+} and Fe^{3+} ions and their preferred sites distribution [33]. Moreover, the reduction in the exchange interactions of Fe^{3+}-O-Fe^{3+}

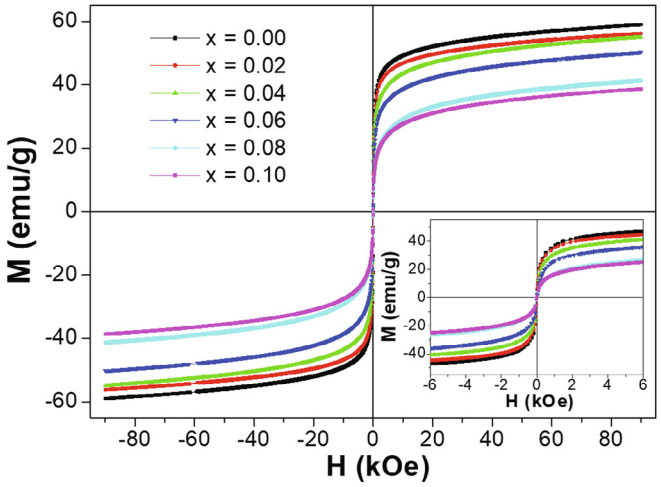

Fig. 7. M − H curves of $Ni_{0.4}Cu_{0.2}Zn_{0.4}Eu_xFe_{2-x}O_4$ ($0.00 \leq x \leq 0.10$) SNPs performed at room temperature.

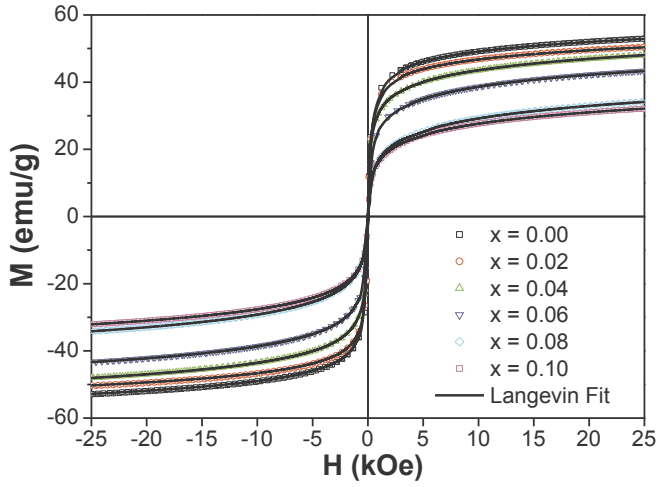

Fig. 8. M − H curves along with Langevin fit (solid lines) for superparamagnetic $Ni_{0.4}Cu_{0.2}Zn_{0.4}Eu_xFe_{2-x}O_4$ ($0.00 \leq x \leq 0.10$) SNPs at room temperature.

by substituting some Fe^{3+} ions with Eu^{3+} ions could provoke a decline in M_s. Indeed, three types of interactions among A and B sites, that are A–A, B–B and A–B, are existing in spinel ferrites wherein the strongest among them is the A-B sublattice interactions [40,41]. Generally, RE ions preferentially occupy the B sites as a consequence of their larger ionic radii [42]. Accordingly, the substitution of Eu^{3+} ions, which have lower magnetic moments than that of Fe^{3+} ions, at B sites will diminish the magnetization. n_B showed similar tendency of M_s evolution with respect to Eu^{3+} content. The non-substituted sample displays the highest M_s and n_B values at room temperature. With increasing × content, M_s and n_B is diminishing. The decrease in n_B is caused by the fact that the A–B exchange interactions are weakened [43].

Magnetization versus temperature (M-T)

Fig. 10 presents the measurements of magnetization versus temperature (M-T) under zero-field-cooling (ZFC) and field-cooling (FC) modes for x = 0.02, 0.06 and 0.10 SNPs. M_{ZFC} and M_{FC} were achieved starting from RT down to very low temperature of about 10 K and under magnetic field of 100 Oe. A splitting and large irreversibility among ZFC and FC curves is seen in various prepared samples, which are characteristic of MNPs. It is observed that the magnitudes of M_{ZFC} and M_{FC} reduced with increasing Eu^{3+} content, which is in good agreement with M − H measurements. For different prepared NPs, the FC magnetization increases gradually with dropping the temperature and then remains constant (plateau-like behavior) below a certain critical temperature. According to numerous investigations [43,44], $M_{FC}(T)$ increases continuously for SPM NPs. However, the slow increase or plateau-type at lower temperature is a signature of a change in magnetic behavior.

On the other hand, numerous investigations reported that the appearance of a peak in ZFC curves is related to T_B (blocking temperature), wherein MNPs are having SP behaviour beyond T_B and transit to FM (ferromagnetic) behavior lower T_B [45]. The enlarged views of $M_{ZFC}(T)$ curves, as shown in Fig. 10(b,d,f), indicated a broad maximum at T_B for various prepared NPs. This indicates a transition from SPM to FM behavior below T_B. The large peak around at $T \sim T_B$ in ZFC curves indicated a widen energy barrier distribution where the thermal activation is surmounted the magnetic anisotropy barrier, leading to fluctuation in the magnetization. Moreover, it is clear that the T_B is influenced by the Eu^{3+} substitution. The x = 0.02 sample displays a T_B around 25 K. T_B increases with the increase in Eu^{3+} substituting content. It increases to about 225 K and 250 K for x = 0.06 and 0.10 compositions, respectively. Generally, the variation in T_B is inversely dependent to the evolutions in particles size. In the present study, it is obvious that the increase in T_B values is continued by a reduction in crystallite size.

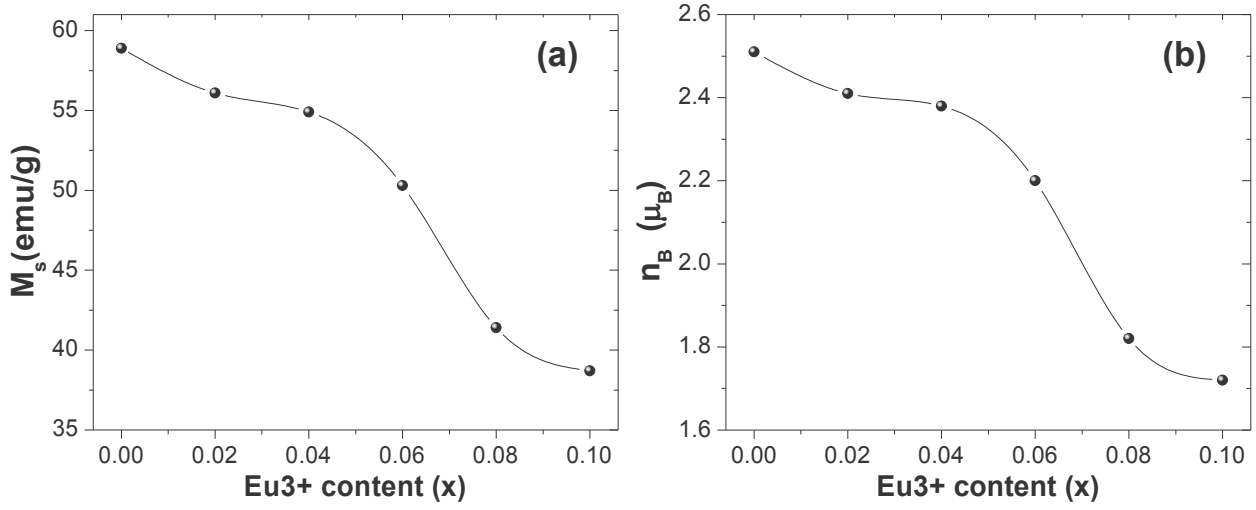

Fig. 9. Variations in M_s and n_B values of $Ni_{0.4}Cu_{0.2}Zn_{0.4}Eu_xFe_{2-x}O_4$ ($0.00 \leq x \leq 0.10$) SNPs at room temperature with respect to Eu^{3+} content.

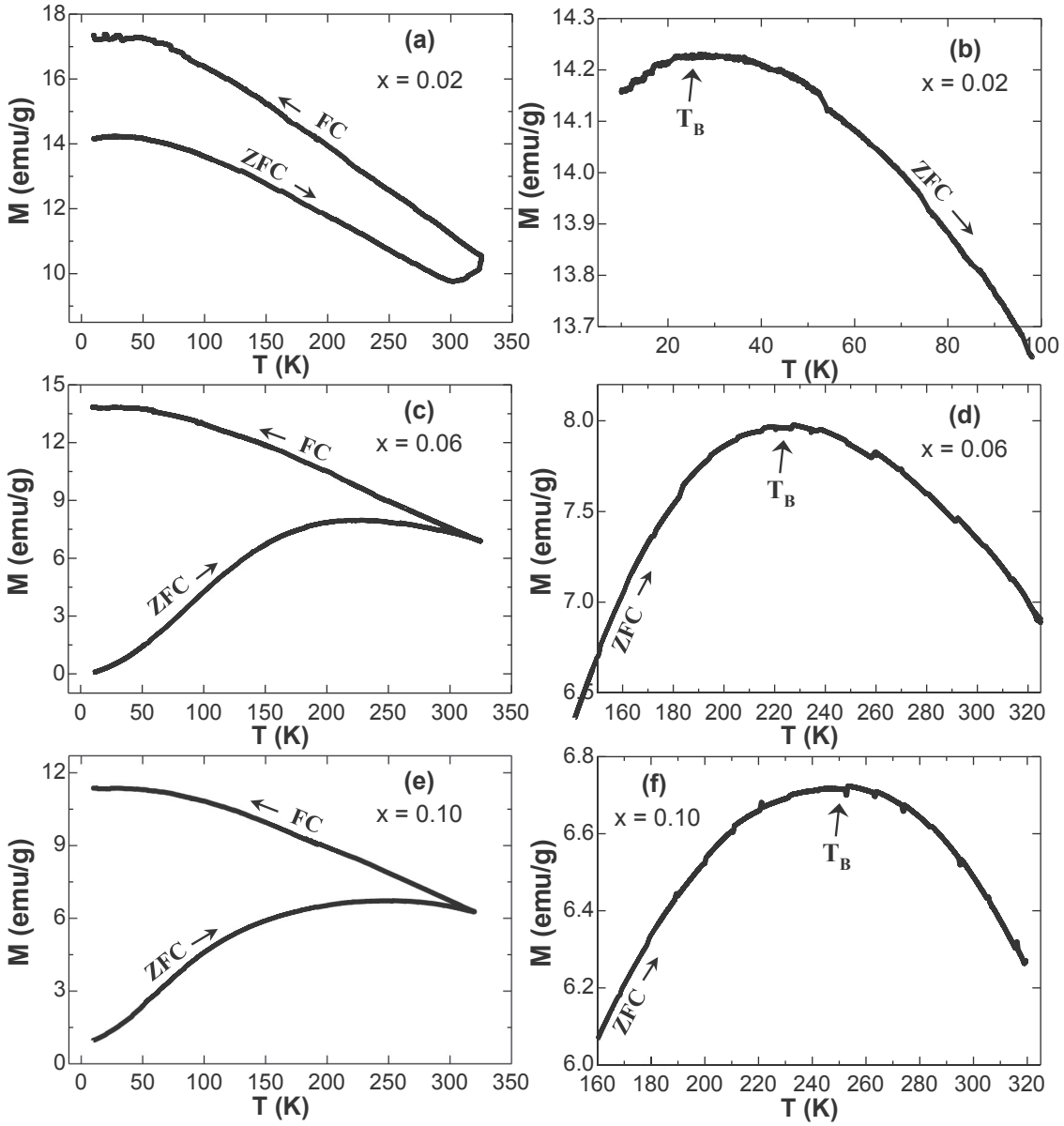

Fig. 10. Magnetization versus temperature (M − T) curves performed with zero-field-cooling (ZFC) and field-cooling (FC) modes of $Ni_{0.4}Cu_{0.2}Zn_{0.4}Eu_xFe_{2-x}O_4$ SNPs for x = 0.02 (a,b), 0.06 (c,d) and 0.10 (e,f).

Electrical and dielectric analysis

Many nanostructured spinel ferrites offer us a useful productive outcome in many technological fields such as microwave absorbers, hyperthermia, nonvolatile memory device, ferro-fluids, medical diagnostics and super capacitor applications [46–49]. Therefore, complex impedance analysis provides a powerful method for evaluating the electrical and dielectric properties of many spinel ferrites. It is evident that each of the parameters related to electrical and dielectric traits is important in examining many characteristic properties of most of the substituted spinel structures. These important parameters show that they make some contribution to dielectric properties depending on grains size influence and interface characteristics according to grain-grain boundaries. Thus, the various properties include the dielectric constant, the conductivity and the dielectric loss as functions of frequency, temperature and many single or multiple substitutional ratios. The contribution to conductivity can arise from two characteristics; the first contributes to dc conductivity owing to the "*band conduction mechanism*" and the second to the ac conductivity caused by "*hopping conduction mechanism*", which is the result of the transport of a particular element between identical ions occurring in various valence states. Such curvilinear behavior implies the result of power law dependency. Therefore, the characterization of the NiCuZn ferrites with an Eu ionic substitution between x = 0.00 to 0.10 have been studied extensively for both frequency and temperature variation under the 3D plot formalism.

AC conductivity

The *ac* conductivities of the $Ni_{0.4}Cu_{0.2}Zn_{0.4}Fe_{2-x}Eu_xO_4$ (x = 0.00 – 0.10) SNPs and also of the non-substituted one as a reference are depicted in the 3D graphs of Fig. 11 versus both frequencies of up to 3 MHz and temperatures of up to 120 °C. Substituted samples generally show that the ac conductivity varies depending on a power law dependency for almost all Eu ion substitution ratios except the lowest of x = 0.02. When the conductivity variation is examined in case of temperature increase for each Eu^{3+} content, it has been noticed that while

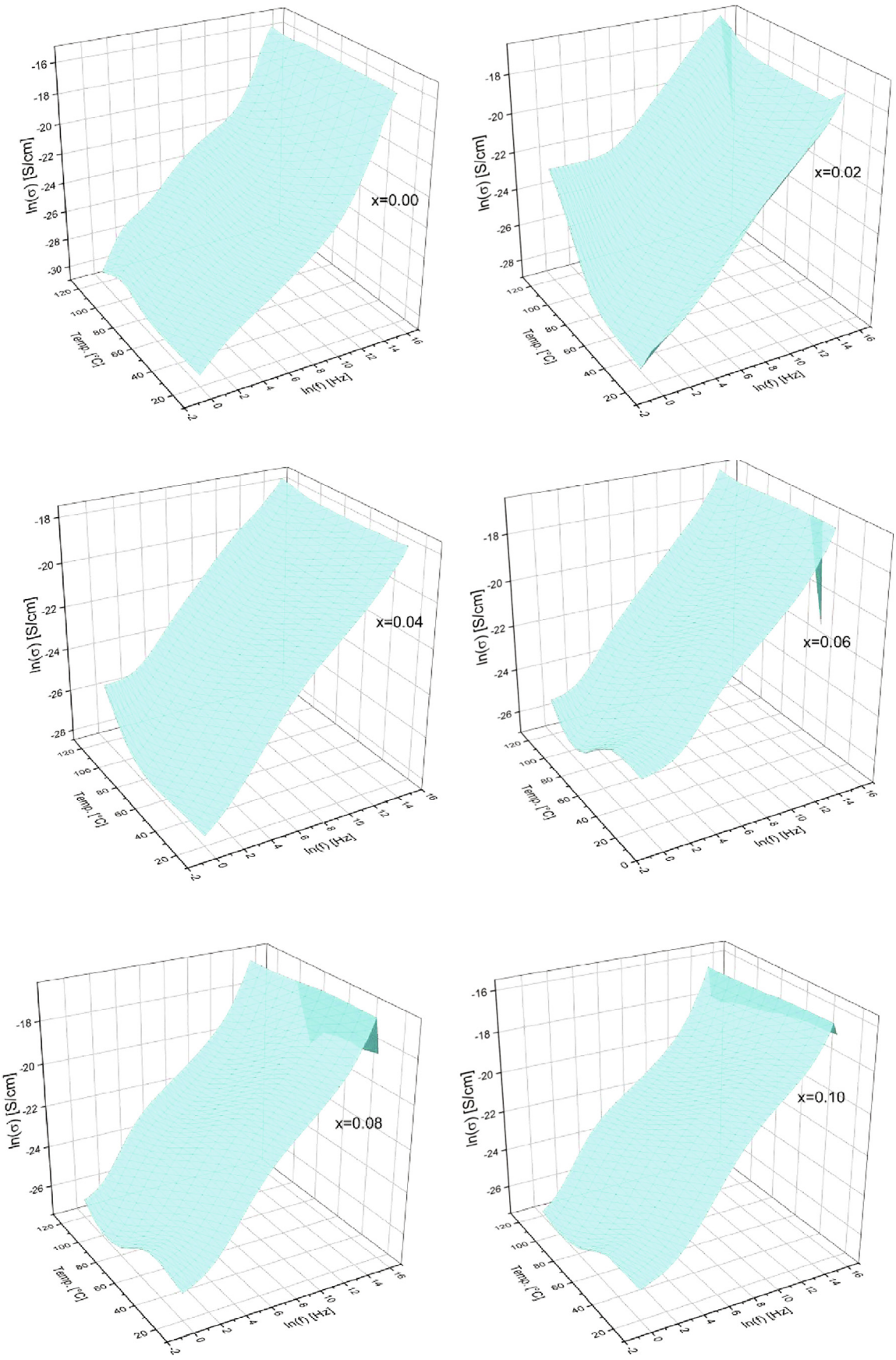

Fig. 11. The 3D representations of AC conductivity of a variety of $Ni_{0.4}Cu_{0.2}Zn_{0.4}Eu_xFe_{2-x}O_4$ ($0.00 \leq x \leq 0.10$) SNPs.

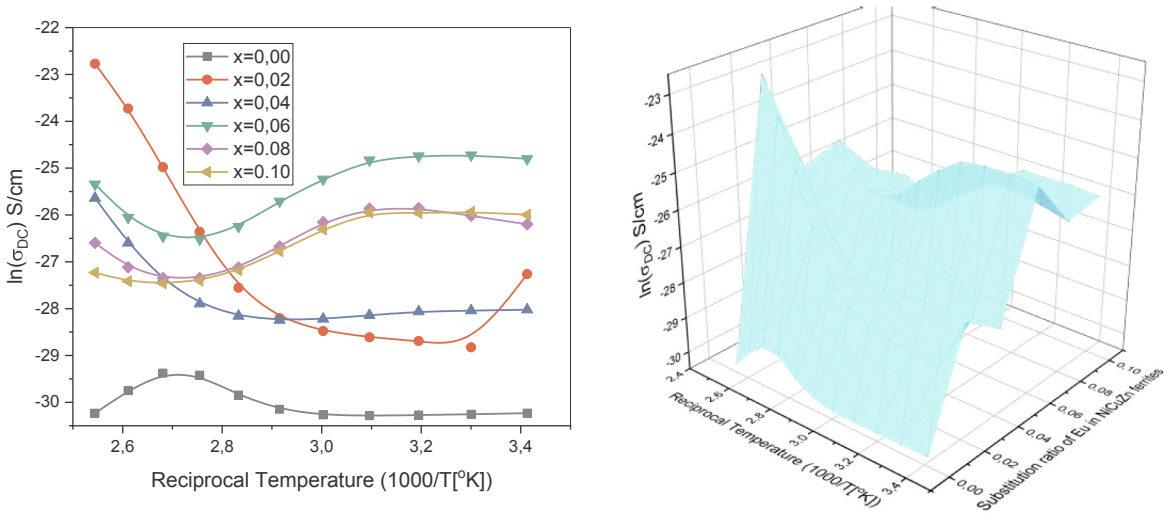

Fig. 12. 2D and 3D Arrhenius plots of DC conductivity of $Ni_{0.4}Cu_{0.2}Zn_{0.4}Eu_xFe_{2-x}O_4$ ($0.00 \leq x \leq 0.10$) SNPs.

the conductivity value fluctuates in lower frequencies and higher substitution ratios (x = 0.06; 0.08; 0.10), it increases in lower frequencies and lower substitution ratios (x = 0.00; 0.02; 0.04). However, it is seen that ac conductivity of all samples in high frequency range is almost temperature independent except for the ratio of x = 0.02. Here, clicks and sharp drops in the highest frequency boundary region due to instrumental measurement limitations can be ignored.

DC conductivity

Both 2D and 3D Arrhenius plots of dc conductivity for $Ni_{0.4}Cu_{0.2}Zn_{0.4}Fe_{2-x}Eu_xO_4$ ($x = 0.00 – 0.10$) SNPs are shown in Fig. 12 for various substitution ratios and for unsubstituted reference ferrites. In Arrhenius plots, the dc conductivity for NiCuZn SPNs first rises, reaches a maximum value and then drops, and then remains constant with increasing reciprocal temperature. However, for highly substituted samples of the ratio x = 0.06, 0.08 and 0.10, the curves first decrease and then increase, after which they remain virtually unchanged. Finally, for less substituted ferrites, such as the ratio of x = 0.02 and 0.04, the dc conductivity decreases almost exponentially with the reciprocal temperature. Maximum variation in dc conductivity is observed to be around the substitution ratio of x = 0.02. Such dc conductivity behavior gives us some advantages that the activation energies of NiCuZn SNPs can be easily modified by varying the substitution ratio of Eu-ions. The conduction mechanism can also be explained as follows; any substitution may be considered as a charge carrier, possibly due to O2p electrons or holes in spinel NiCuZn SNPs of crystallite nanoparticles. Another additional contribution to the variation in the Arrhenius plots can originate from the interfacial effects between the grains and grain boundaries for poly-crystallites of ferrite nanoparticles, owning to a significant effect on the fluctuation of conduction mechanism [23].

Dielectric constant

The general tendency of dielectric constant (ε') is the decrease with frequency, which is a common characteristic of ferrites. [50,51]. So, the dielectric constant of $Ni_{0.4}Cu_{0.2}Zn_{0.4}Fe_{2-x}Eu_xO_4$ ($x = 0.00 – 0.10$) SNPs is shown in Fig. 13 in 3-D plot versus frequency and temperature. Unsubstituted and low $Ni_{0.4}Cu_{0.2}Zn_{0.4}Eu_xFe_{2-x}O_4$ SNPs (x = 0.02, 0.04) show us a different trend over temperature rise. However, highly substituted samples, such as x = 0.06, 0.08 and 0.10, show more regular tendencies for increase in temperature and frequency as well as substitution ratios. In the entire frequency and temperature range studied here, the dielectric constant does not have a significant dependence on the higher Eu ion substitution ratios such as x = 0.06, 0.08 and 0.10. For the x = 0.00 and 0.02 ferrites, the dielectric constant was found to be temperature dependent at low and medium frequencies, but at higher frequencies it was found to be temperature independent. It should be also emphasized that the dielectric constant of the unsubstituted and substituted NiCuZn ferrites is almost temperature independent at high frequency due to the time delay in reaction to the change of the applied electric field.

This behaviour of ε' with frequency able to be clarified based on the Maxwell-Wagner polarization model, which explains that conduction mechanism leads to similar hopping process between ferric and ferrous ions [52]. The hopping frequency of the charge carriers follows the externally applied electric field at low frequencies, resulting in a rise in ε'. However, the hopping frequency of the charge carriers cannot follow the applied electric field at higher frequencies, and therefore ε' is reduced owing to random dipolar orientation. Often, dielectric constant behaviour can also be defined based on Koop's phenomenological model [53,54].

Dielectric loss

The dielectric loss curve of $Ni_{0.4}Cu_{0.2}Zn_{0.4}Fe_{2-x}Eu_xO_4$ ($x = 0.00 – 0.10$) SNPs shows us some type of extraordinary absorption tendencies in the mid frequency range in the first graph of Fig. 14, whereas the loss effect in the mid frequency region is eliminated for Eu ion-substituted NiCuZn SNPs for the rest. However, some inverted peaks for the ratios of x = 0.02 and 0.06, and some inverted wall-like tendencies along temperature at a certain frequency for x = 0.08 and 0.10 compositions in the loss seem to be due to intensive absorption at certain frequency, which may result from the local inhomogeneity and the Eu ionic diffusion in NiCuZn SNPs. Again, for x = 0.02 ferrite, the loss parameter decreases and then increases with an increasing temperature. For other highly substituted NiCuZn SNPs, the dielectric loss almost fluctuates with temperature at low frequencies but remains less variable across temperature ranges at high frequencies.

Dissipation factor

The dielectric tangent loss of $Ni_{0.4}Cu_{0.2}Zn_{0.4}Fe_{2-x}Eu_xO_4$ ($x = 0.00 – 0.10$) SNPs is shown in 3-D graphs of Fig. 15 of the relation between temperature (T) and frequency (*f*). It can be clearly seen that the frequency and temperature dependencies of tangent loss as a dissipation factor are observed to be more complicated for each of the Eu ion substituted and unsubstituted NiCuZn SNPs. For the unsubstituted ferrite, the tangential loss value is highly dependent on the *f*, although the T dependence is quite low. For the low Eu ion-substituted samples of x = 0.02 and 0.04, both own a peak rise at low *f* at high T. However, for

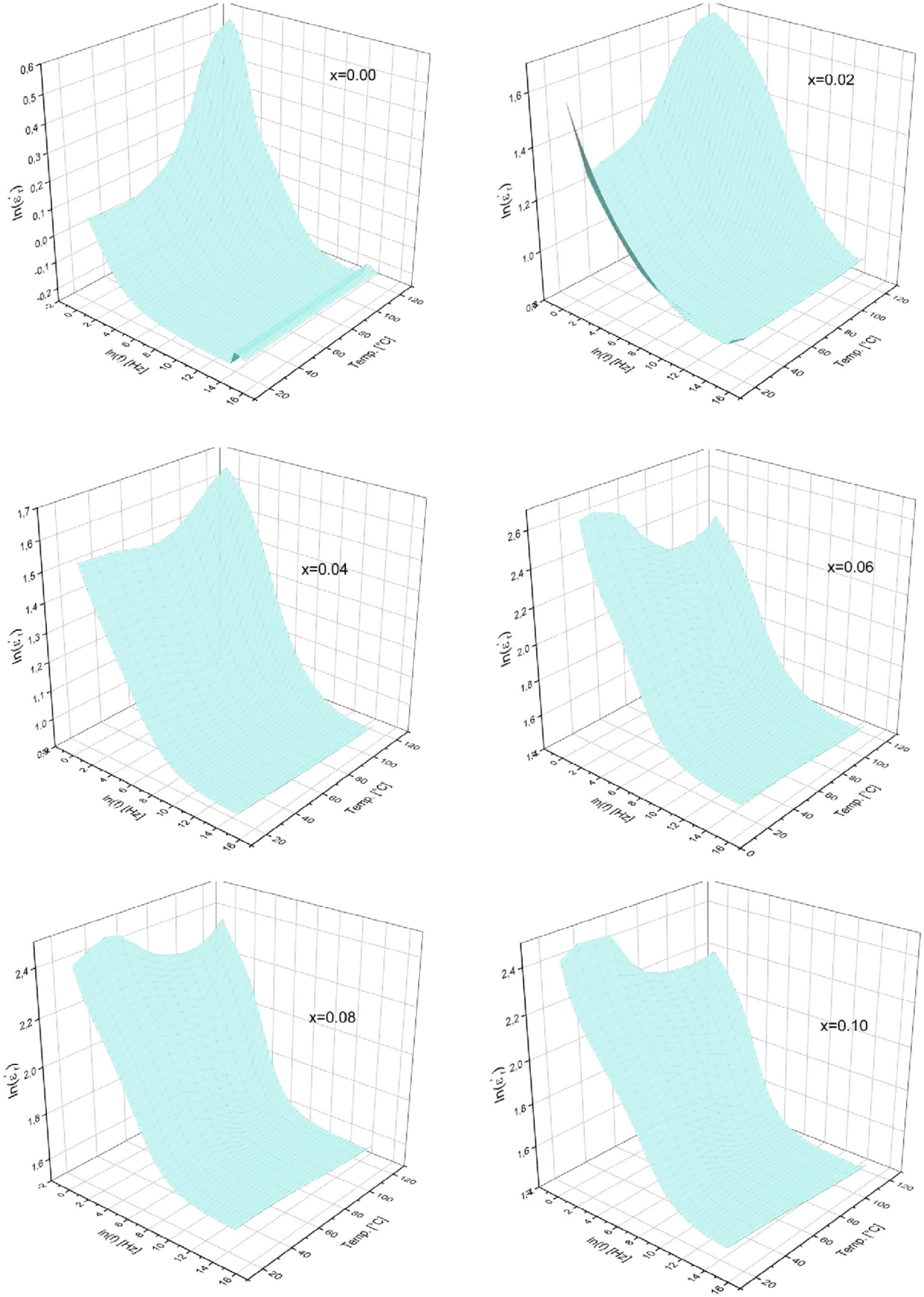

Fig. 13. The 3D representations of dielectric constant of a variety of $Ni_{0.4}Cu_{0.2}Zn_{0.4}Eu_xFe_{2-x}O_4$ ($0.00 \leq x \leq 0.10$) SNPs.

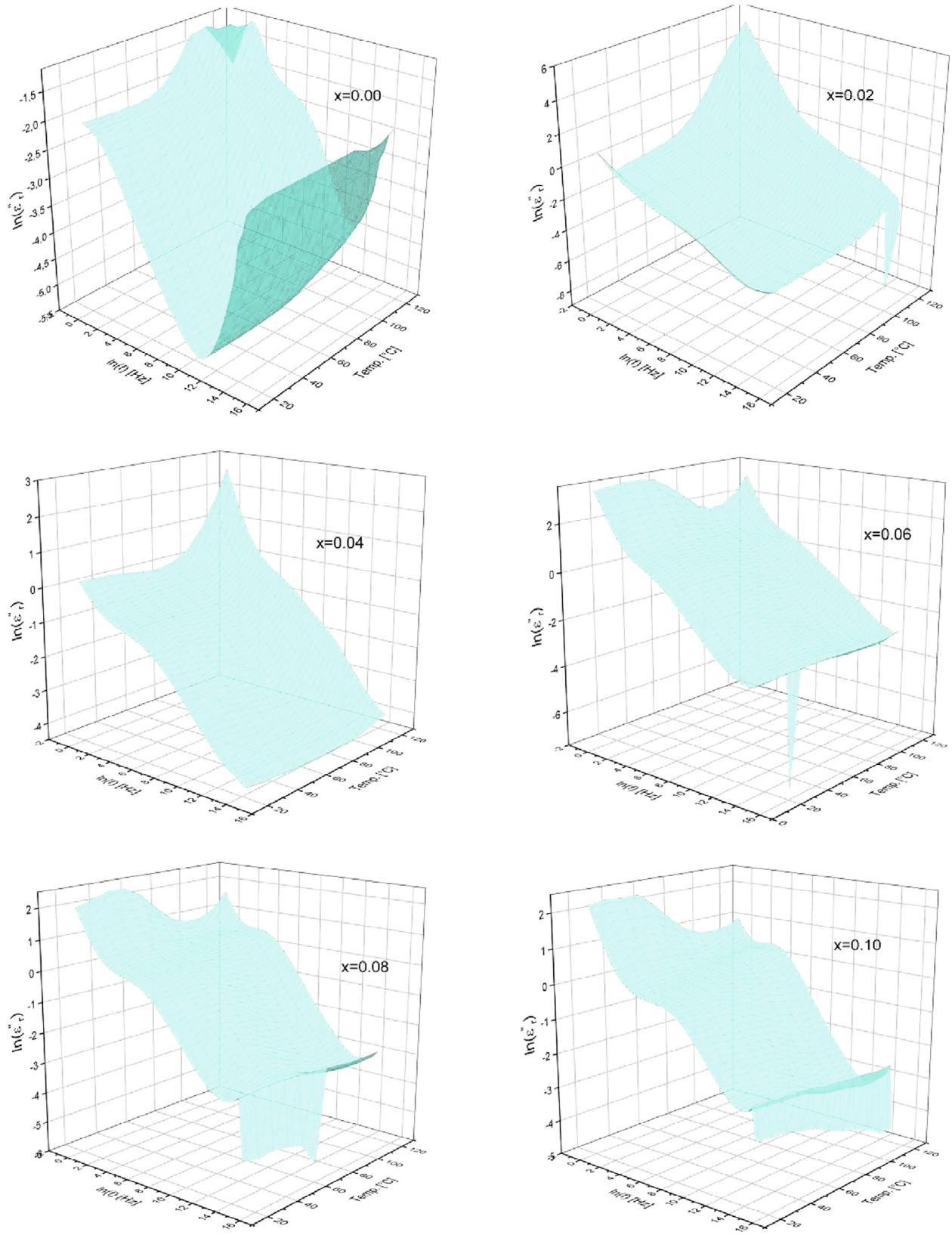

Fig. 14. The 3D representations of dielectric loss of a variety of $Ni_{0.4}Cu_{0.2}Zn_{0.4}Eu_xFe_{2-x}O_4$ ($0.00 \leq x \leq 0.10$) SNPs.

the highly Eu ion-substituted SNPs such as 0.06, 0.08 and 0.10, all of them presents maximum values at low frequencies at low and medium temperatures range and drops sharply with the increase of f reducing the peak value with the reduction of substitution ratios at low f in the high temperature. At high f, all the substituted SNPs show the lowest dissipation factor unlike unsubstituted NiCuZn SNPs as depicted in Fig. 15. The incorporation of Eu ions as a replacement for ferric ions becomes so important in NiCuZn SNPs. The rise in the molar ratio of Eu ions causes a decrease in dielectric tangent loss since the Eu ions decreases the grain's conductance by limiting the hopping mechanism

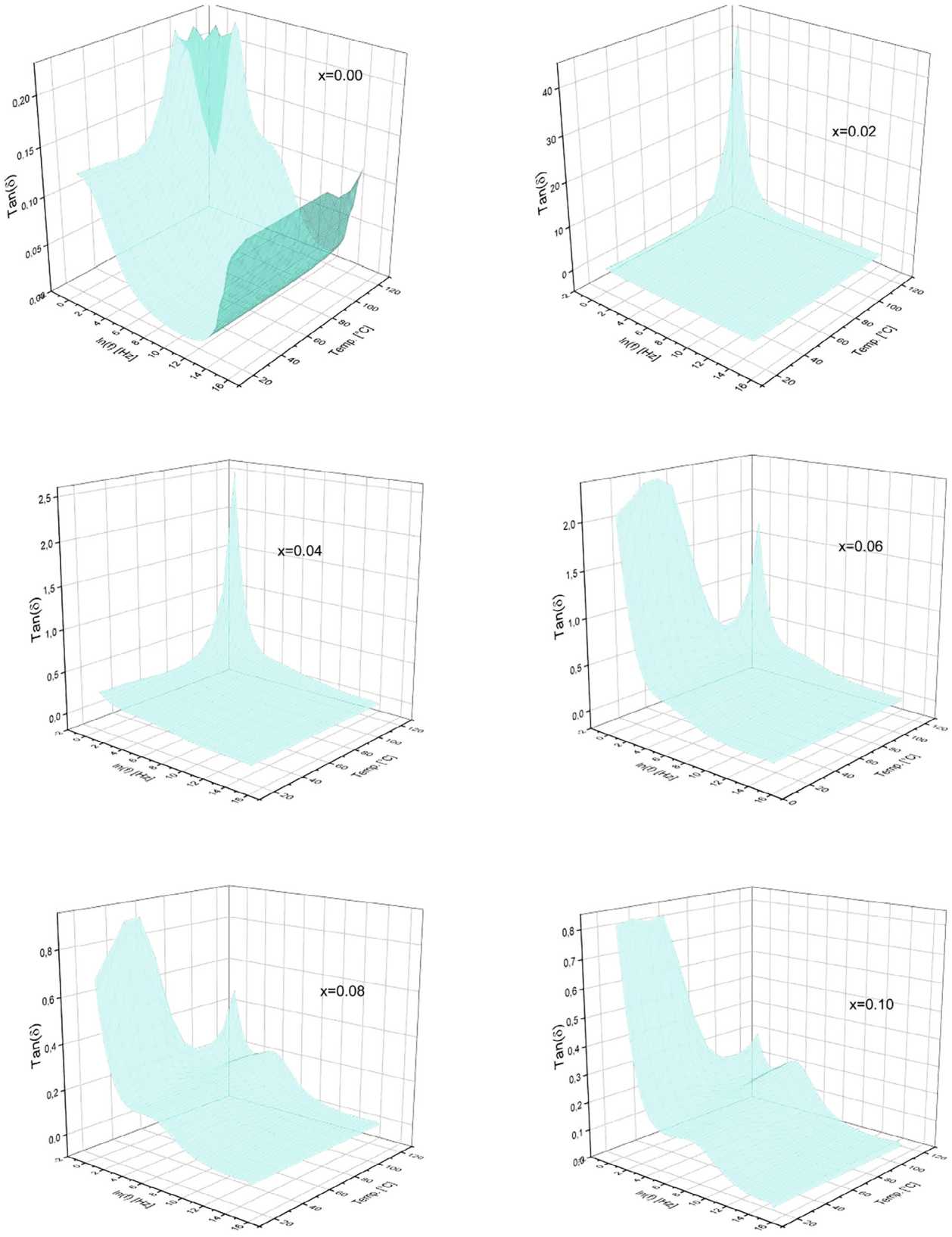

Fig. 15. The 3D representations of dielectric tangent loss of $Ni_{0.4}Cu_{0.2}Zn_{0.4}Eu_xFe_{2-x}O_4$ ($0.00 \leq x \leq 0.10$) SNPs.

between the ferrous ion and the ferric ion. Furthermore, the small polarons produced in the ferrites can be considered to contribute to the polarization leading to abnormal dielectric behaviour. The creation of small polarons is possible in nanocrystallites because of the narrow conductive band [55,56]. Furthermore, the resonance leading to the relaxation peak occurs when the hopping frequency of the localized charge carriers is equal to the externally applied electric field frequency. High frequency characteristics and heat-resonance losses make these materials beneficial for hyperthermia and medical diagnosis. The value of the maximum tangential loss at low f makes Eu^{3+} ion

substituted NiCuZn SNPs useful in various devices operating at medium *f*.

Conclusion

Single phase $Ni_{0.4}Cu_{0.2}Zn_{0.4}Fe_{2-x}Eu_xO_4$ (x = 0.00 – 0.10) SNPs have been fabricated via ultrasonic irradiation approach. Rietveld refinement of XRD patterns approved the formation NiCuZn SNPs and showed a rise in the lattice parameters with rising the amount of substitution ions. %DR investigations revealed that direct E_g values lie in the semiconductor bandgap range of 1.86–1.90 eV for different $Ni_{0.4}Cu_{0.2}Zn_{0.4}Fe_{2-x}Eu_xO_4$ (x = 0.00 – 0.10) SNPs. Eu^{3+} ion doping process slightly changes the E_g magnitudes. $M-H$ measurements indicated a superparamagnetic behavior at room temperature and below a certain critical temperature noted as blocking temperature (T_B) a transition from superparamagnetic to ferromagnetic behavior was observed. M_s decreased with increasing Eu^{3+} substituting content. The diminish in magnetization is ascribed to reduction in crystallites size, lower magnetic moments of Eu^{3+} (3.4 μ_B) compared to that of Fe^{3+} ions (5 μ_B), cations distribution, and weakening of A-B super-exchange interactions. In the investigation of electrical and dielectric traits of Eu ions substituted NiCuZn ferrites, it was observed that (i) ac conductivity was in compliance with the power exponent laws, (ii) the activation energies fluctuate with Eu ion substitution ratios as in the La and Y ions substitutes, and (iii) dielectric constant and dielectric loss decreased sharply with increasing frequencies under a variety of power law formalism. Both frequency dependency and heat-resonance losses make Eu ion-substituted NiCuZn SNPs useful for hyperthermia and medical diagnosis. The value of the maximum tangential loss at low frequencies and high temperature makes such ferrites also useful in a variety of devices operating at medium frequencies. The frequency dependence of dielectric functions was interpreted by Koop's models based on Maxwell-Wagner theory.

CRediT authorship contribution statement

Y. Slimani: Conceptualization, Methodology, Investigation, Writing - review & editing, Supervision. **B. Unal:** Investigation. **M.A. Almessiere:** Conceptualization, Methodology, Investigation, Supervision. **A. Demir Korkmaz:** Writing - review & editing. **Sagar E. Shirsath:** Investigation. **Ghulam Yasin:** Investigation. **A.V. Trukhanov:** Investigation. **A. Baykal:** Conceptualization, Methodology, Supervision.

Declaration of Competing Interest

The authors declare that they have no known competing financial interests or personal relationships that could have appeared to influence the work reported in this paper.

References

[1] Slimani Y, Almessiere MA, Nawaz M, Baykal A, Akhtar S, Ercan I, et al. Effect of bimetallic (Ca, Mg) substitution on magneto-optical properties of $NiFe_2O_4$ nanoparticles. Ceram Int 2019;45:6021–9.

[2] Almessiere MA, Slimani Y, Güner S, Baykal A, Ercan I. Effect of dysprosium substitution on magnetic and structural properties of $NiFe_2O_4$ nanoparticles. J. Rare Earths 2019;37:871–8.

[3] Ikram S, Jacob J, Mahmood K, Ali A, Amin N, Rehman U, et al. Influence of Ce^{3+} substitution on the structural, electrical and magnetic properties of $Zn_{0.5}Mn_{0.43}Cd_{0.07}Fe_2O_4$ spinel ferrites. Phys B 2020;580:411764.

[4] Ikram S, Jacob J, Arshad MI, Mahmood K, Ali A, Sabir N, et al. Tailoring the Structural, Magnetic and Dielectric properties of Ni-Zn-$CdFe_2O_4$ spinel ferrites by the substitution of Lanthanum ions. Ceram Int 2019;45:3563.

[5] Ikram S, Imran Arshad M, Mahmood K, Ali A, Amin N, Ali N, et al. magnetic and dielectric study of La^{3+} substituted $Cu_{0.8}Cd_{0.2}Fe_2O_4$ ferrite nanoparticles synthesized by the co-precipitation method. J Alloys Compd 2018;769:1019.

[6] Tatarchuk T, Myslin M, Mironyuk I, Bououdina M, Pędziwiatr T, Gargula R, et al. Synthesis, morphology, crystallite size and adsorption properties of nanostructured Mg–Zn ferrites with enhanced porous structure. J. Alloys Compd 2020;819:152945.

[7] Tatarchuk T, Mironyuk I, Kotsyubynsky V, Shyichuk A, Myslin M, Boychuk V. Structure, morphology and adsorption properties of titania shell immobilized onto cobalt ferrite nanoparticle core. J Mol Liquids 2020;297:111757.

[8] Starko I, Tatarchuk T, Bououdina M. La-doped $Ni_{0.5}Co_{0.5}Fe_2O_4$ nanoparticles: effect of cobalt precursors on structure and morphology. Mol Cryst Liq Cryst 2018;674:110–9.

[9] Verma R, Kane SN, Tiwari P, Modak SS, Tatarchuk T, Mazaleyrat F. Ni addition induced modification of structural, magnetic properties and antistructural modeling of $Zn_{1x}Ni_xFe_2O_4$ (x = 0.0 - 1.0) nanoferrites. Mol Cryst Liq Cryst 2018;674:130–41.

[10] Ahmed MA, Hassan HE, Eltabey MM, Latka K, Tatarchuk TR. Mössbauer spectroscopy of $Mg_xCu_{0.5-x}Zn_{0.5}Fe_2O_4$ (x = 0.0, 0.2 and 0.5) ferrites system irradiated by γ-rays. Phys B 2018;530:195–200.

[11] Sharifi I, Shokrollahi H, Amiri S. Ferrite-based magnetic nanofluids used in hyperthermia applications. J Magn Magn Mater 2012;324(6):903–15.

[12] Kefeni KK, Msagati TA, Mamba BB. Ferrite nanoparticles: synthesis, characterisation and applications in electronic device. Mater Sci Eng, B 2017;215:37–55.

[13] Krishnaveni T, Kanth BR, Raju VSR, Murthy SR. Fabrication of multilayer chip inductors using Ni–Cu–Zn ferrites. J Alloys Compd 2006;414(1):282–6.

[14] Harzali H, Saida F, Marzouki A, Megriche A, Baillon F, Espitalier F, et al. Structural and magnetic properties of nano-sized NiCuZn ferrites synthesized by co-precipitation method with ultrasound irradiation. J Magn Magn Mater 2016;419:50–6.

[15] Slimani Y, Almessiere MA, Korkmaz AD, et al. $Ni_{0.4}Cu_{0.2}Zn_{0.4}Tb_xFe_{2x}O_4$ nanospinel ferrites: Ultrasonic synthesis and physical properties. Ultrason Sonochem 2019;59:104757.

[16] Shinde TJ, Gadkari AB, Vasambekar PN. Magnetic properties and cation distribution study of nanocrystalline Ni–Zn ferrites. J Magn Magn Mater 2013;333:152–5.

[17] Azhagushanmugam SJ, Suriyanarayanan N, Jayaprakash R. Synthesis and Characterization of Nanocrystalline Ni(0.6) Zn(0.4) Fe2O4 Spinel Ferrite Magnetic Material. Phys Procedia 2013;49:44–8.

[18] Hashim M, Alimuddin Shirsath SE, Kumar S, Kumar R, Roy AS, et al. Preparation and characterization chemistry of nano-crystalline Ni–Cu–Zn ferrite. J Alloys Compd 2013;549:348–57.

[19] Saida F, Harzali H, Marzouki A, Mgaidi A, Megriche A. Effect of cobalt substitution on the structural and magnetic properties of nanopowders Ni0.4Cu0.2Zn0.2Fe2 O 4 by hydrothermal method. J Tunisian Chem Soc. 2017;19:26-31.

[20] Eltabey MM, El-Shokrofy KM, Gharbia SA. Enhancement of the magnetic properties of Ni–Cu–Zn ferrites by the non-magnetic Al3+-ions substitution. J Alloys Compd 2011;509(5):2473–7.

[21] Roy PK, Nayak BB, Bera J. Study on electro-magnetic properties of La substituted Ni–Cu–Zn ferrite synthesized by auto-combustion method. J Magn Magn Mater 2008;320(6):1128–32.

[22] Kabbur SM, Waghmare SD, Nadargi DY, Sartale SD, Kambale RC, Ghodake UR, et al. Magnetic interactions and electrical properties of Tb3+ substituted NiCuZn ferrites. J Magn Magn Mater 2019;473:99–108.

[23] Harzali H, Marzouki A, Saida F, Megriche A, Structural Mgaidi A. magnetic and optical properties of nanosized Ni0. 4Cu0. 2Zn0. 4R0. 05Fe1. 95O4 (R= Eu3+, Sm3+, Gd3+ and Pr3+) ferrites synthesized by co-precipitation method with ultrasound irradiation. J Magn Magn Mater 2018;460:89–94.

[24] Nam J-H, Park SJ, Kim WK. Microstructure and magnetic properties of nanostructured NiZnCu ferrite powders synthesized by sol-gel process. IEEE Trans Magn 2003;39(5):3139–41.

[25] Liu F, Ren T, Yang C, Liu L, Wang Ai, Yu J. NiCuZn ferrite thin films for RF integrated inductors 2006. 1403-6 p.

[26] Tauc J, Grigorovici R, Vancu A. Optical properties and electronic structure of amorphous germanium. Physica Status Solidi 1966;15:627–37.

[27] Güner S, Amir Md, Geleri M, Sertkol M, Baykal A. Magneto-Optical Properties of Mn^{3+} substituted Fe_3O_4 Nanoparticle. Ceram Int 2015;41(9):10915–22.

[28] Slimani Y, Baykal A, Amir Md, Güngüneş H, Guner S, El Sayed HS, et al. Substitution effect of Cr^{3+} on hyperfine interactions, magnetic and optical properties of Sr-hexaferrites. Ceram Int 2018;44:15995–6004.

[29] Auwal IA, Güngüneş H, Güner S, Shirsath Sagar E, Sertkol M, Baykal A, et al. magneto-optical properties and cation distribution of $SrBi_xLa_xY_xFe_{12-3x}O_{19}$ ($0.0 \leq x \leq 0.33$) hexaferrites. Mater Res Bull 2016;80:263–72.

[30] Laurent S, Forge D, Port M, Roch A, Robic C, Elst LV, et al. Magnetic Iron Oxide Nanoparticles: Synthesis, Stabilization, Vectorization, Physicochemical Characterizations, and Biological Applications. Chem Rev 2008;108:2064–110.

[31] Almásy L, Creanga D, Nadejde C, Rosta L, Pomjakushina E, Ursache-Oprisan M. Wet milling versus co-precipitation in magnetite ferrofluid preparation. J Serb Chem Soc 2015;80:367–76.

[32] Almessiere MA, Slimani Y, Kurtan U, Guner S, Sertkol M, Shirsath Sagar E, et al. magnetic, optical properties and cation distribution of nanosized $Co_{0.7}Zn_{0.3}Tm_xFe_{2x}O_4$ ($0.0 \leq x \leq 0.04$) spinel ferrites synthesized by ultrasonic irradiation. Ultrason Sonochem 2019;58:104638.

[33] Almessiere MA, Slimani Y, Korkmaz AD, Taskhandi N, Sertkol M, Baykal A, et al. Sonochemical synthesis of Eu^{3+} substituted $CoFe_2O_4$ nanoparticles and their structural, optical and magnetic properties. Ultrason Sonochem 2019;58:104621.

[34] Chaudhari Vivek, Shirsath Sagar E, Mane ML, Kadam RH, Shelke SB, Mane DR, et al. magnetic and electrical properties of $Ni_{0.5}Cu_{0.25}Zn_{0.25}La_xFe_{2-x}O_4$ nanoparticles fabricated by sol–gel method. J Alloys Compd 2013;549:213–20.

[35] Roy PK, Bera J. Electromagnetic properties of samarium-substituted NiCuZn ferrite prepared by auto-combustion method. J Magn Magn Mater 2009;321:247–51.

[36] Liu Feng, Yang Chen, Tianling Ren AZ, Wang Jun Yu, Liu Litian. NiCuZn ferrite thin films grown by a sol–gel method and rapid thermal annealing. J Magn Magn Mater 2007;309:75–9.

[37] Almessiere MA, Slimani Y, Güner S, Baykal A, Ercan I. Effect of dysprosium

substitution on magnetic and structural properties of $NiFe_2O_4$nanoparticles. J Rare Earths 2019. https://doi.org/10.1016/j.jre.2018.10.009.
[38] Almessiere MA, Slimani Y, Güner S, Nawaz M, Baykal A, Aldakheel F, et al. Magnetic and structural characterization of Nb^{3+}-substituted $CoFe_2O_4$ nanoparticles. Ceram Int 2019;45:8222–32.
[39] Murugesan C, Chandrasekaran G. Impact of Gd^{3+} substitution on the structural, magnetic and electrical properties of cobalt ferrite nanoparticles. RSC Adv 2015;5:73714–25.
[40] Almessiere MA, Slimani Y, Guner S, Nawaz M, Baykal A, Aldakheel F, et al. Effect of Nb substitution on magneto-optical properties of $Co_{0.5}Mn_{0.5}Fe_2O_4$ nanoparticles. J Mol Struct 2019;1195:269–79.
[41] Almessiere MA, Slimani Y, Sertkol M, Khan FA, Nawaz M, Tombuloglu H, et al. Ce–Nd Co-substituted nanospinel cobalt ferrites: an investigation of their structural, magnetic, optical, and apoptotic properties. Ceram Int 2019;45:16147–56.
[42] Almessiere MA, Korkmaz AD, Slimani Y, Nawaz M, Ali S, Baykal A. Magneto-optical properties of Rare Earth metals substituted Co-Zn spinel nanoferrites. Ceram Int 2019;45:3449–58.
[43] Peddis D, Cannas C, Piccaluga G, Agostinelli E, Fiorani D. Surface spin freezing effects on enhanced saturation magnetization and magnetic anisotropy in $CoFe_2O_4$ nanoparticles. Nanotechnology 2010;21:125705.
[44] Chen X, Bedanta S, Petracic O, Kleemann W, Sahoo S, Cardoso S, et al. Superparamagnetism versus superspin glass behavior in dilute magnetic nanoparticle systems. Phys Rev B 2005;72:214436.
[45] Humbe AV, Kounsalye JS, Shisode MV, Jadhav KM. Rietveld refinement, morphology and superparamagnetism of nanocrystalline $Ni_{0.70-x}Cu_xZn_{0.30}Fe_2O_4$ spinel ferrite. Ceram Int 2018;44:5466–72.
[46] Alam RS, Moradi M, Rostami M, Nikmanesh H, Moayedi R, Bai Y. Structural, magnetic and microwave absorption properties of doped Ba-hexaferrite nanoparticles synthesized by co-precipitation method. J Magn Magn Mater 2015;381:1–9.
[47] Wan F, Luo F, Mu Y, Zeng Z, Zhou W. Enhanced mechanical and microwave-absorption properties of $SiC_f/AlPO_4$ composite with PIP–SiC interphase and the MWCNTs filler. J Ceram Int 2015;41:9957–65.
[48] Harzali H, Saida F, Marzouki A, Megriche A, Baillon F, Espitalier F, et al. Structural and magnetic properties of nanosized NiCuZn ferrites synthesized by co-precipitation method with ultrasound irradiation. J Magn Magn Mater 2016;419:50–6.
[49] Sadiq I, Naseem S, Ashiq MN, Khan MA, Niaz S, Rana MU. Structural and dielectric properties of doped ferrite nanomaterials suitable for microwave and biomedical applications. Prog Chem Org Nat Prod in Natural Science: Materials International 2015;25:419–24.
[50] Almessiere MA, Ünal B, Slimani Y, Korkmaz AD, Baykal A, Ercan I. Electrical properties of La^{3+} and Y^{3+} ions substituted $Ni_{0.3}Cu_{0.3}Zn_{0.4}Fe_2O_4$ nanospinel ferrites. Results Phys 2019;15:102755–65.
[51] M.A. El-Hiti, Electrical and Dielectric Properties of NixMg1 − xFe2O4, J. Phys. III 6 (1996) 1307-1313.
[52] Bakıs Y, Auwal IA, Ünal B, Baykal A. Maxwell-Wagner relaxation in grain boundary of $BaBi_xLa_xY_xFe_{123x}O19$ ($0.0 < x < 0.33$) hexaferrites. Compos B 2016;99:248–56.
[53] Reddy AVR, Mohan GR, Ravinder D, Boyanar BS. High-frequency dielectric behaviour of polycrystalline zinc substituted cobalt ferrites. J Mater Sci 1999;34:3169–76.
[54] Bakış Y, Auwal IA, Ünal B, Baykal A. Conductivity and dielectric properties of $SrLa_xBi_xY_xFe_{12-3x}O_{19}$ ($0.0 \leq x \leq 0.33$) hexaferrites. Ceram Int 2016;42:11780–95.
[55] Bao J, Zhou J, Yue Z, Li L, Gui Z. Dielectric behaviour of Mn-substituted Co_2Z hexaferrites. J Magn Magn Mater 2002;250:131–7.
[56] Purushotham Y, Reddy PV. Charge transport and conduction mechanism of some substituted strontium W-type hexagonal ferrites. Int J Mod Phys B 1996;10:319–36.